

Aeroacoustic limit-cycles obtained by blowing across a bottle's top

E. Boujo,* C. Bourquard, Y. Xiong, and N. Noiray†

CAPS Laboratory, Department of Mechanical and Process Engineering, ETH Zürich, 8092 Zürich, Switzerland

(Dated: December 19, 2020)

Blowing across the opening of a bottle to produce sound is an entertaining and yet intriguing activity. We investigate experimentally this phenomenon, and quantify the common observation that a distinct tone is obtained for a large enough blowing velocity and for a finite range of blowing angles. We extract the spatio-temporal evolution of the acoustic energy production and dissipation from the flapping shear layer at the bottle neck. We develop a simple analytical model of a linear acoustic oscillator (the bottle) subject to non-linear stochastic forcing (from the turbulent jet). This Van der Pol oscillator model allows us to explain the stochastic fluctuations of the acoustic amplitude, on both sides of the Hopf bifurcation, which result from a competition between linear growth rate induced by the coherent unsteady vortex force, random forcing induced by the turbulence and non-linear saturation of the coherent flapping motion of the jet. We use the associated adjoint Fokker-Planck equation to reveal the deterministic potential well and the stochastic forcing intensity that governs these random fluctuations of the acoustic amplitude. This system identification approach can be used in a wide range of phenomena exhibiting stationary self-sustained oscillations.

Introduction. – Bottles are the archetype of Helmholtz resonators (HRs) and their acoustics has been long understood [1, 2]. They are analogous to mechanical mass-spring-damper oscillators: the air inside the bottle's neck acts as an oscillating mass and the air inside the bottle's cavity acts as a spring, while damping arises from acoustic visco-thermal losses at the inner wall and acoustic radiation losses at the neck opening. Helmholtz-like resonators are used in many different contexts to absorb acoustic energy, e.g. for improving room acoustics, decreasing noise pollution (aeroengine liners, car mufflers), or preventing thermoacoustic instabilities in rocket engines or gas turbines. Many articles deal with the linear and nonlinear response of HRs to acoustic forcing [3–8], and with their aeroacoustic properties when submitted to bias/grazing flow through/over their neck (see [9–12] for experimental studies, and [13–18] for theoretical/numerical studies). They have also attracted attention for investigations on sub-wavelength focusing [19, 20], synchronization [21] and energy harvesting [22].

When subject to a flow, HRs may exhibit self-sustained oscillations, as observed in daily life and engineering applications, e.g. bottle whistling (from its simplest form to sophisticated multi-bottle organs), music (e.g. the ocarina and some primitive instruments), or ground transportation (when an open train window or car sunroof leads to buffeting or wind throb). These aeroacoustic instabilities result from a constructive feedback between the acoustic oscillations in the resonator and the associated hydrodynamic response in the neck region. Indeed, acoustic energy is pumped from the kinetic energy of the flow because jets, mixing layers and other shear flows can amplify flow perturbations [23]; this energy transfer has also been recently exploited to realize experimentally an aeroacoustic \mathcal{PT} -symmetric system [24]. Although seemingly simple, these aeroacoustic instabilities involve the generation, transport, amplification and saturation of coherent vorticity fluctuations in a turbu-

lent flow (over spatio-temporal scales of several orders of magnitude). These mechanisms strongly depend on the geometry and flow conditions, so their modeling and prediction are challenging. Finally, the stochastic aspects associated with flow turbulence are seldom investigated or even taken into account.

In this study, we bring the stochastic forcing from the turbulence into focus. We derive a simple model of Van der Pol (VdP) oscillator that combines (i) the acoustics of the HR, (ii) the non-linear forcing from the shear layer, and (iii) the stochastic forcing induced by turbulence. We then identify the oscillator's governing parameters from experimental single-microphone measurements performed over a range of mean flow conditions. The output-only parameter identification method crucially relies on the stochastic nature of the forcing that drives the system away from its deterministic equilibrium, causing it to explore a wide region of the phase space, thus revealing precious information about its dynamics and, ultimately, about its governing parameters.

Experimental setup. – The air jet produced by a circular pipe of diameter $d = 5$ mm impinges the neck (inner diameter $D = 17.2$ mm) of a 330 mL beer bottle (Fig. 1(a)). The jet bulk velocity $U = 12 - 24 \pm 0.1$ m/s is $4\dot{m}/\bar{\rho}\pi d^2$, where $\bar{\rho}$ is the air density and \dot{m} the mass flow. The Reynolds number $Re = \bar{\rho}dU/\mu = 4000 - 8000$ (with μ the air dynamic viscosity) is large enough for the jet to be fully turbulent. A precision rotary table allows the jet angle to be varied in the range $\theta = 0 - 90 \pm 0.1^\circ$ around a rotation axis centered on the trailing edge of the upstream rim of the bottle neck. The distance from the pipe outlet to the rotation axis is 37 mm. The acoustic pressure in the bottle is recorded with a microphone GRAS 46BD-S2.

Whether whistling occurs or not, depends on the jet velocity U and angle θ . Figure 1(b) shows, for a whistling case ($U = 22$ m/s, $\theta = 45^\circ$), measurements of streamwise velocity $u_x = \mathbf{u} \cdot \mathbf{e}_x$ and spanwise vortic-

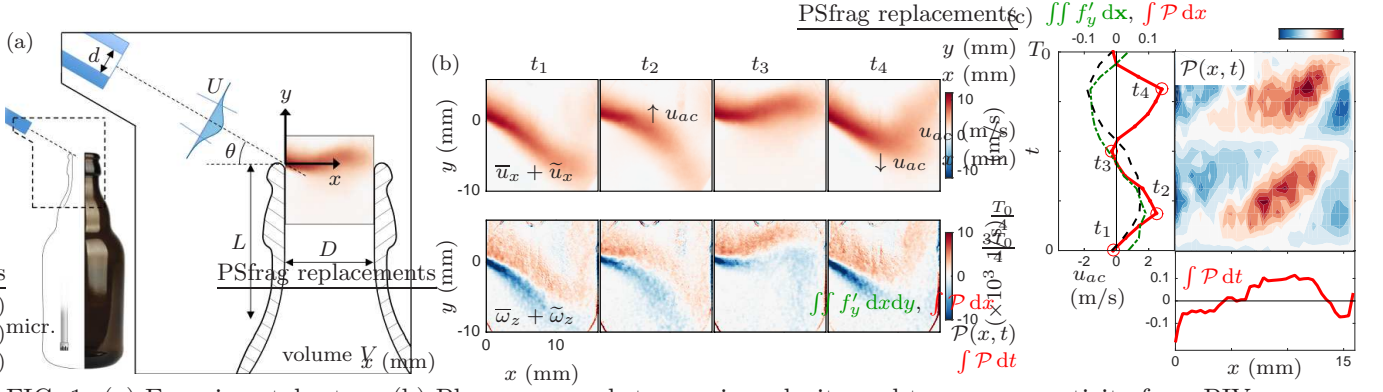


FIG. 1: (a) Experimental setup. (b) Phase-averaged streamwise velocity and transverse vorticity from PIV measurements ($U=22$ m/s, $\theta = 45^\circ$). (See movie in the Supplemental Material [25].) (c) Acoustic power density \mathcal{P} as a function of streamwise location and time; temporal and vertical integrals of \mathcal{P} ; time evolution of the acoustic velocity u_{ac} and space-integrated fluctuating vertical force f'_y .

ity $\omega_z = \boldsymbol{\omega} \cdot \mathbf{e}_z = \partial_x u_y - \partial_y u_x$ obtained in the neck in the plane of symmetry of the jet $z = 0$ with particle image velocimetry (PIV) after phase averaging (keeping time-average fields \bar{u}_x , $\bar{\omega}_z$, and coherent fluctuations \tilde{u}_x , $\tilde{\omega}_z$, while removing incoherent fluctuations) at different phases of the acoustic cycle. PIV is performed by seeding the jet with DEHS particles (mean diameter $1 \mu\text{m}$), illuminating the plane with a 0.5 mm laser sheet (double-pulse, 532 nm, 2×6 mJ at 10 kHz), and collecting the particles Mie scattering with a high-speed CMOS camera. These fields illustrate the jet structure and its transverse motion at the whistling frequency.

The bottle and the jet constitute an aeroacoustic system, where coupling occurs through mutual interaction: the turbulent jet acts as a forcing upon the acoustic field of the HR, and acoustic fluctuations in the bottle neck exert a feedback forcing on the jet. Thus, whistling is a self-sustained aeroacoustic oscillation, where part of the kinetic energy from the turbulent jet is pumped into the acoustic field. It is possible to leverage this PIV data further by considering Howe's analogy [26], which expresses how the fluctuating component of the Lamb vector $\boldsymbol{\omega} \times \mathbf{u}$ induces a vortex force $\mathbf{f}'(x, y, t) = \bar{\rho}(\boldsymbol{\omega} \times \mathbf{u})'$ that does work on the acoustic field: Figure 1(c) shows the acoustic power density given to or taken from the acoustic field across the neck during an oscillation cycle,

$$\mathcal{P}(x, t) = \int \mathbf{f}' \cdot \mathbf{u}_{ac} dy = - \int \bar{\rho}(\boldsymbol{\omega} \times \mathbf{u})' \cdot \mathbf{u}_{ac} dy, \quad (1)$$

where the spatial distribution of the acoustic velocity \mathbf{u}_{ac} is computed with a Helmholtz solver, and its temporal evolution is calibrated from vorticity-free regions of the flow (see Supplemental Material [25]). Importantly, the aeroacoustic coupling inside the neck is three dimensional, so the map generated from the center-plane velocity field only gives qualitative information. Also, it does not reflect the production from the unstable base flow (steady solution of the incompressible Navier–Stokes equations), because \mathcal{P} is processed from limit-cycle data,

where the effective gain from the nonlinear aeroacoustic feedback balances the linear acoustic damping (viscothermal and radiation losses) (see Supplemental Material [25]). That said, it is enlightening to observe that, for this limit cycle ($U=22$ m/s, $\theta = 45^\circ$), regions near the upstream and downstream rims are, on average, dissipating acoustic energy, while the central region is producing acoustic energy, as shown by the power density integrated over one acoustic period, denoted $\int \mathcal{P} dt$. The instantaneous net effect over the neck width, $\int \mathcal{P} dx$, is positive at all times. This acoustic power production is the result of a good synchronization between the vertical acoustic velocity $u_{ac} = \mathbf{u}_{ac} \cdot \mathbf{e}_y$ and the vertical force $f'_y = \mathbf{f}' \cdot \mathbf{e}_y$ (approximately equal to $-\bar{\rho}(\omega_z u_x)'$ given the system geometry), yielding production when u_{ac} is directed both outward and inward.

Observations. – Varying the jet velocity and angle leads to distinct behaviors. Figure 2(a) shows time signals of acoustic pressure $p(t)$ (red) recorded for $\theta = 30^\circ$, $U = 17$ and 19 m/s, and their envelope $A(t)$ (black) extracted with the Hilbert transform. For $U=19$ m/s (intense whistling), the signal is characterized by large-amplitude harmonic oscillations (aeroacoustic frequency $\omega_a/2\pi$), with a slowly varying envelope (see inset) whose random fluctuations result from the stochastic forcing of the turbulent jet. The stationary probability density function (PDF) $P_\infty(p)$ of the acoustic pressure is bimodal with symmetric peaks, and the PDF $P_\infty(A)$ of the envelope has its peak shifted away from zero with an inflection point on its tail. This is typical of limit-cycle oscillations (see also the joint PDF $P_\infty(p, \dot{p}/\omega_a)$). For $U=17$ m/s (no whistling), the limit cycle disappears and one retrieves the dynamics of a noise-driven linearly stable oscillator. $P_\infty(p)$ is unimodal with a peak centered around zero. As shown in Fig. 2(b), whistling occurs in a tongue-shaped region in the U - θ plane and acoustic pressure fluctuations inside the bottle are stronger for larger velocities $U \geq 18$ m/s and intermediate angles $10^\circ \leq \theta \leq 50^\circ$, reaching up to $p_{\text{rms}} = 1.4$ mbar (sound pressure level 135 dB) in

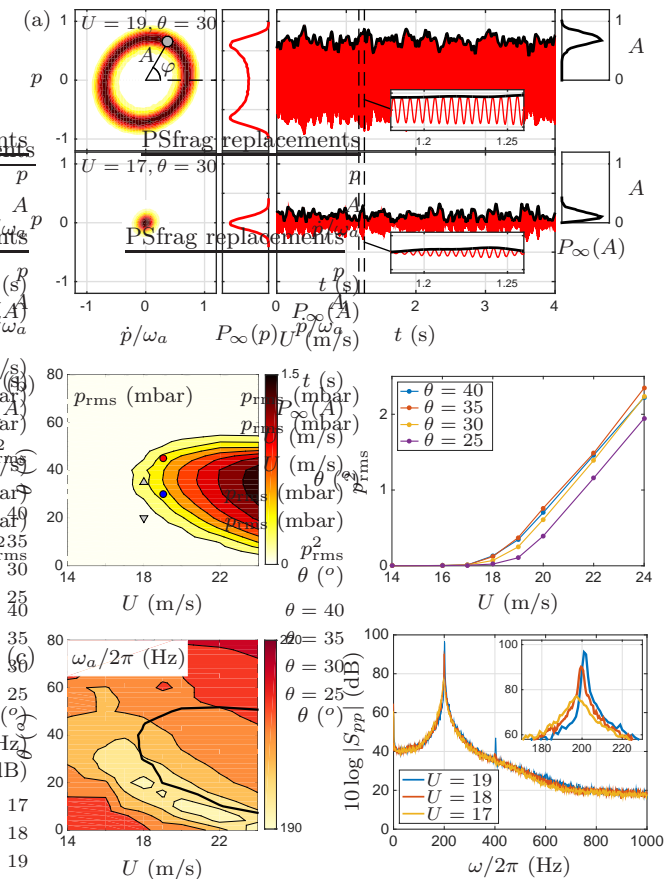


FIG. 2: (a) Sample acoustic pressure signal $p(t)$ inside the bottle, corresponding envelope $A(t)$, and their respective stationary PDF $P_\infty(p)$ and $P_\infty(A)$. (b) Acoustic pressure fluctuations p_{rms} vs. jet velocity U and jet angle θ . Circles and triangles show conditions of Fig. 4 and S5, respectively. Scaling $p_{\text{rms}}^2 \propto U - U_c$ above the onset of whistling at a critical velocity U_c . (c) Aeroacoustic frequency vs. U and θ (thick line: stability limit $\nu = 0$; see Fig. 3). Frequency spectra for increasing jet velocities ($\theta = 30^\circ$).

the investigated range. Above the onset of whistling at a critical velocity U_c , acoustic pressure fluctuations increase like $p_{\text{rms}} \propto \sqrt{U - U_c}$. Over the whole range of considered velocities and angles, acoustic pressure signals are almost harmonic and power spectra exhibit a dominant peak at $f_a \simeq 195 - 210$ Hz (Fig. 2(c)), consistent with the natural frequency $f_0 = c\sqrt{S/V}L_{\text{eq}}/2\pi$ of a HR of equivalent neck length $L_{\text{eq}} = 47$ mm, neck cross-section area $S = \pi D^2/4 = 2.3 \times 10^{-4}$ m² and total volume $V = 3.3 \times 10^{-4}$ m³ in air (speed of sound $c = 340$ m/s at ambient temperature). See Supplemental Material [25] for details.

Physical model. – We model the aeroacoustic system as a white-noise-driven VdP oscillator (see Supplemental Material [25]). The dynamics of the acoustic pressure $p(t)$ inside the bottle is governed by

$$\ddot{p} + \omega_0^2 p = (2\nu - \kappa p^2)\dot{p} + \xi(t), \quad (2)$$

with $\omega_0 = 2\pi f_0$ the oscillator's natural angular frequency, $\xi(t)$ a white Gaussian noise of intensity Γ (delta-correlated: $\langle \xi \xi_\tau \rangle = \Gamma \delta(\tau)$) corresponding to an idealized random forcing from jet turbulence, ν the linear growth rate resulting from the combination of stabilizing damping mechanisms (radiation and visco-thermal losses) and constructive/destructive aeroacoustic feedback between the jet and the bottle, whose non-linear component appears in the saturation term proportional to κ . The envelope $A(t)$ and phase $\varphi(t)$ are slowly varying compared to the period $2\pi/\omega_0$, so we write $p(t) = A(t) \cos(\omega_0 t + \varphi(t))$ and use deterministic and stochastic averaging [27] to reduce (2) to a system of equations for the phase dynamics $\dot{\varphi} = \chi(t)/A$ and amplitude dynamics

$$\dot{A} = \nu A - \frac{\kappa}{8} A^3 + \frac{\Gamma}{4\omega_0^2 A} + \zeta(t), \quad (3)$$

with $\zeta(t)$ and $\chi(t)$ two independent white Gaussian noises of intensity $\Gamma/2\omega_0^2$ ($\langle \zeta \zeta_\tau \rangle = \langle \chi \chi_\tau \rangle = (\Gamma/2\omega_0^2)\delta(\tau)$). The Langevin equation (3) is independent of the phase and reads in a potential form $\dot{A} = -\mathcal{V}'(A) + \zeta(t)$, with $\mathcal{V}(A) = -\nu A^2/2 + \kappa A^4/32 - (\Gamma/4\omega_0^2) \ln(A)$. The evolution of $P(A, t)$ is governed by the Fokker-Planck equation (FPE) associated with (3):

$$\partial_t P = -\partial_A (D^{(1)} P) + \partial_{AA} (D^{(2)} P), \quad (4)$$

where the drift and diffusion coefficients $D^{(1)}, D^{(2)}$ (first two terms of the Kramers-Moyal (KM) expansion [27, 28]) are linked to (3):

$$D^{(1)}(A) = \nu A - \frac{\kappa}{8} A^3 + \frac{\Gamma}{4\omega_0^2 A}, \quad D^{(2)} = \frac{\Gamma}{4\omega_0^2}. \quad (5)$$

The stationary PDF $P_\infty(A) = \lim_{t \rightarrow \infty} P(A, t)$ is directly determined by the KM coefficients:

$$P_\infty(A) = \mathcal{N} \exp \frac{\int D^{(1)}(A)}{D^{(2)}} = \mathcal{N} \exp \left(-\frac{\mathcal{V}(A)}{\Gamma/4\omega_0^2} \right) \quad (6)$$

with \mathcal{N} a normalization factor such that $\int_0^\infty P_\infty(A) dA = 1$. Note that the mode A_m (most probable amplitude, where $P_\infty(A)$ is maximum and $D^{(1)}(A) = 0$) differs from the deterministic amplitude $A_{\text{det}} = \sqrt{8\nu/\kappa}$.

Parameter identification. – We now proceed with the identification of the system's governing parameters ν, κ, Γ , solely from measured signals of acoustic pressure under stationary conditions. Input-output identification is not possible when the input cannot be measured or when the system cannot be driven arbitrarily. The challenging task of output-only identification can be undertaken with a variety of methods, e.g. Kalman filters [29], modal identification [30], reduced-order modeling [31], empirical dynamic modeling [32], sparse identification [33], and estimation of the KM coefficients [34, 35]. The latter has been applied to analyze stochastic data sets in many systems: turbulence [36, 37], financial markets [38], traffic

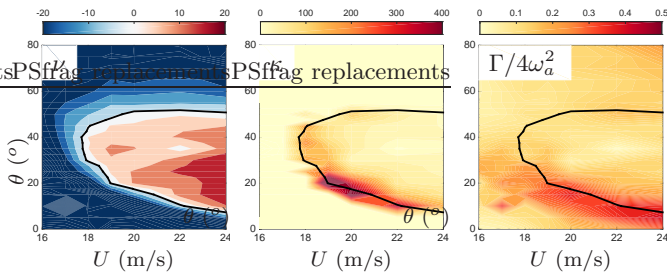


FIG. 3: Parameters of the stochastic VdP oscillator (2) and stochastic amplitude equation (3), identified with an adjoint-based optimization method. Black line: stability limit $\nu = 0$.

flow [39], epileptic brain dynamics [40], earthquakes [41], wind-energy [42]. Here we use a version where robustness and accuracy are improved by minimizing the difference between finite-time KM coefficients calculated from time signals and those calculated with the adjoint FPE [43–45]. We used 30 s stationary time traces for each coordinate (U, θ) . The identification results (Fig. 3) show that the oscillator is linearly unstable ($\nu > 0$) for larger velocities and intermediate angles, and linearly stable otherwise, with the stability boundary $\nu = 0$ following closely the contour ($p_{\text{rms}} \simeq A \simeq 0.4$ mbar) of the tongue-shaped region in Fig. 2(b). κ and Γ are maximum along the stability boundary and for smaller angles. This significant asymmetry strikingly contrasts with the rms map (Fig. 2(b)). Uncovering the physical mechanisms responsible for the dependency of ν, κ, Γ on U and θ will require further investigation with numerical simulations and PIV measurements of the unsteady flow.

Similar statistic, different dynamics. – We have shown that different stationary statistics of the stochastic acoustic oscillator correspond to different governing parameters. We now turn our attention to the effect of these parameters on the system’s *dynamic* behavior. We note that different sets of parameters may result in similar acoustic levels (Figs. 2-3) and similar PDFs. For instance, for $U = 19$ m/s, both $\theta = 30^\circ$ and 45° (red and blue circles in Fig. 2(b)) lead to $p_{\text{rms}} = 0.50$ mbar and to similar stationary PDFs (Fig. 4(c)), while system identification yields $\{\nu, \kappa, \Gamma/4\omega_a^2\} = \{9.0, 148, 0.17\}$ and $\{4.9, 83, 0.10\}$ respectively. $\theta = 30^\circ$ results in a larger growth rate and a stronger saturation, leading to a well of the potential $\mathcal{V}(A)$ that is deeper than for $\theta = 45^\circ$. In parallel, the identified noise intensity is higher too, and the system is able to explore wider regions of $\mathcal{V}(A)$ (Fig. 4(b)). The net result is that the two systems have the same stationary *statistic*. However, their *dynamics* differ. Figure 4(a) shows $P(A, t)$ when starting from a non-equilibrium PDF centered around low amplitudes. Both systems relax to the same $P_\infty(A)$ but at different rates, because the underlying potentials have different depths. For any stationary condition, U and θ have a strong influence on the dynamics of the system on its

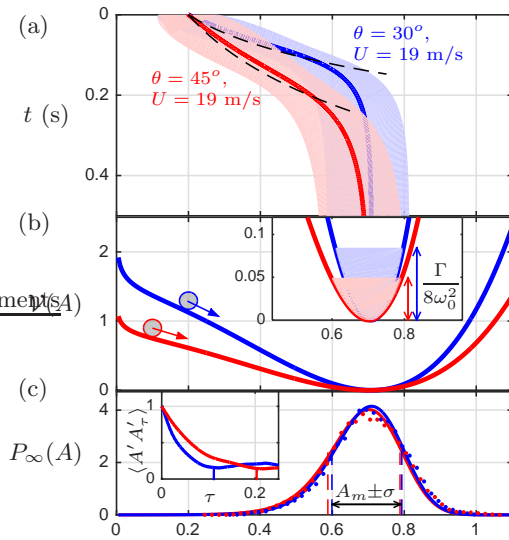


FIG. 4: (a) Time evolution $P(A, t)$ for two conditions (circles in Fig. 2(b)) exhibiting different transient dynamics and yet leading to the same stationary statistic. Numerical simulation of the FPE with the identified ν, κ, Γ from the adjoint-based identification. Colored areas: $P(A, t)$ larger than a fixed given value. The most probable amplitude $A_m(t)$ (thick lines) compares well with the exponential growth $A_m(0)e^{\nu t}$ (dashes). (b) Identified potential $\mathcal{V}(A)$. Inset: detail of the well around A_m . Colored areas: typical potential height $\Gamma/8\omega_0^2$ reached when the system visits amplitudes in the range $A_m \pm \sigma$ (one standard deviation from the most probable amplitude). (c) $P_\infty(A)$: experimental measurements (symbols) and analytical expression with the identified parameters (solid lines). Inset: normalized autocorrelation of the fluctuations $A' = A - \bar{A}$. (Dashes: characteristic time $1/\nu$.)

way to the limit cycle.

Conclusion. – We have shown that, when blowing across a bottle’s top with appropriate velocity and angle, the self-sustained large-amplitude periodic jet motion induces production of acoustic energy in both phases of the acoustic cycle, and the resulting aeroacoustic limit cycle is well described by a simple VdP oscillator with additive stochastic forcing. We identified under stationary conditions the underlying potential well and stochastic forcing intensity by computing the finite-time transition moments of the acoustic pressure envelope and by solving the adjoint FPE. This model-based identification is useful in order to disentangle deterministic and stochastic effects in the many systems that exhibit stochastic dynamics but cannot be controlled.

This work was supported by Repower and the ETH Zurich Foundation.

* eboujo@ethz.ch

† noirayn@ethz.ch

- [1] H. L. F. Helmholtz, *On the sensations of tone as a physiological basis for the theory of music* (Longmans, Green, 1875).
- [2] J. W. S. Rayleigh, *The theory of Sound* (Dover, 1896).
- [3] A. Cummings, *Applied Acoustics* **5**, 161 (1972).
- [4] A. Cummings, *Journal of Sound and Vibration* **31**, 331 (1973).
- [5] R. L. Panton and J. M. Miller, *The Journal of the Acoustical Society of America* **57**, 1533 (1975).
- [6] P. A. Monkewitz and N.-M. Nguyen-Vo, *Journal of Fluid Mechanics* **151**, 477 (1985).
- [7] D. K. Singh and S. W. Rienstra, *Journal of Sound and Vibration* **333**, 3536 (2014).
- [8] V. Achilleos, O. Richoux, and G. Theocharis, *The Journal of the Acoustical Society of America* **140**, EL94 (2016).
- [9] B. E. Walker and A. F. Charwat, *The Journal of the Acoustical Society of America* **72**, 550 (1982).
- [10] R. L. Panton and J. M. Miller, *The Journal of the Acoustical Society of America* **58**, 800 (1975).
- [11] R. Khosropour and P. Millet, *The Journal of the Acoustical Society of America* **88**, 1211 (1990).
- [12] S. Frikha, P. Y. Hennion, and S. Boukhari, *The Journal of the Acoustical Society of America* **105**, 1186 (1999).
- [13] M. S. Howe, *Journal of Sound and Vibration* **45**, 427 (1976).
- [14] D. Innes and D. G. Crighton, *Journal of Sound and Vibration* **131**, 323 (1989).
- [15] D. G. Crighton and D. Innes, *The Journal of the Acoustical Society of America* **69**, S81 (1981).
- [16] R. Ma, P. Slaboch, and S. Morris, *Journal of Fluid Mechanics* **623**, 1 (2009).
- [17] M. Meissner, *Journal of Sound and Vibration* **256**, 382 (2002).
- [18] X. Dai, X. Jing, and X. Sun, *Physics of Fluids* **27**, 057102 (2015).
- [19] S. Zhang, L. Yin, and N. Fang, *Phys. Rev. Lett.* **102**, 194301 (2009).
- [20] F. Lemoult, M. Fink, and G. Lerosey, *Phys. Rev. Lett.* **107**, 064301 (2011).
- [21] M. Abel, K. Ahnert, and S. Bergweiler, *Phys. Rev. Lett.* **103**, 114301 (2009).
- [22] F. Liu, A. Phipps, S. Horowitz, K. Ngo, L. Cattafesta, T. Nishida, and M. Sheplak, *The Journal of the Acoustical Society of America* **123**, 1983 (2008).
- [23] P. G. Drazin and W. H. Reid, *Hydrodynamic Stability*, 2nd ed. (Cambridge University Press, Cambridge, 2004).
- [24] Y. Aurégan and V. Pagneux, *Phys. Rev. Lett.* **118**, 174301 (2017).
- [25] See Supplemental Material at - URL will be inserted by publisher - for details about Howe's analogy for vortex sound, the derivation of the stochastic oscillator, and an estimation of its natural frequency and acoustic damping.
- [26] M. Howe, *Journal of Sound and Vibration* **70**, 407 (1980).
- [27] R. Stratonovich, *Topics in the Theory of Random Noise*, Vol. 2 (New York: Gordon & Breach, 1967).
- [28] H. Risken, *The Fokker-Planck Equation* (Springer-Verlag, 1984).
- [29] R. E. Kalman, *Journal of Basic Engineering* **82**, 35 (1960).
- [30] S. Nagarajaiah and B. Basu, *Earthquake Engineering and Engineering Vibration* **8**, 583 (2009).
- [31] C. W. Rowley and S. T. M. Dawson, *Annu. Rev. Fluid Mech.* **49**, 387 (2017).
- [32] H. Ye, R. J. Beamish, S. M. Glaser, S. C. H. Grant, C. Hsieh, L. J. Richards, J. T. Schmute, and G. Sugihara, *Proc Natl Acad Sci USA* **112**, E1569 (2015).
- [33] S. L. Brunton, J. L. Proctor, and J. N. Kutz, *Proc Natl Acad Sci USA* **113**, 3932 (2016).
- [34] F. Böttcher, J. Peinke, D. Kleinhans, R. Friedrich, P. G. Lind, and M. Haase, *Phys. Rev. Lett.* **97**, 090603 (2006).
- [35] R. Friedrich, J. Peinke, M. Sahimi, and M. R. R. Tabar, *Physics Reports* **506**, 87 (2011).
- [36] R. Friedrich and J. Peinke, *Phys. Rev. Lett.* **78**, 863 (1997).
- [37] C. Renner, J. Peinke, R. Friedrich, O. Chanal, and B. Chabaud, *Phys. Rev. Lett.* **89**, 124502 (2002).
- [38] R. Friedrich, J. Peinke, and C. Renner, *Phys. Rev. Lett.* **84**, 5224 (2000).
- [39] S. Kriso, J. Peinke, R. Friedrich, and P. Wagner, *Physics Letters A* **299**, 287 (2002).
- [40] J. Prusseit and K. Lehnertz, *Phys. Rev. Lett.* **98**, 138103 (2007).
- [41] P. Manshour, S. Saberi, M. Sahimi, J. Peinke, A. F. Pacheco, and M. R. Rahimi Tabar, *Phys. Rev. Lett.* **102**, 014101 (2009).
- [42] P. Milan, M. Wächter, and J. Peinke, *Phys. Rev. Lett.* **110**, 138701 (2013).
- [43] S. Lade, *Physics Letters A* **373**, 3705 (2009).
- [44] C. Honisch and R. Friedrich, *Physical Review E* **83**, 066701 (2011).
- [45] E. Boujo and N. Noiray, *Proceedings of the Royal Society A: Mathematical, Physical and Engineering Science* **473** (2017).

Aeroacoustic limit-cycles obtained by blowing across a bottle's top (Supplemental Material)

S1. DERIVATION OF THE UNFORCED OSCILLATOR MODEL

We first focus on the acoustic-only system (bottle without impinging jet), before moving to the aero-acoustic system (bottle and jet). The first and second derivatives with respect to time of fluctuating fields q' are denoted \dot{q}' and \ddot{q}' . Assuming that the bottle neck is subject to a time-harmonic fluctuating pressure difference $p'_1 - p'_2 = \Re[(\tilde{p}_1 - \tilde{p}_2)e^{i\omega t}]$ between its inner and outer terminations, that it is acoustically compact (i.e. its length L and diameter D are small with respect to the acoustic wavelength $\lambda = 2\pi c/\omega$) and that the resulting flow is irrotational and inviscid, the momentum balance for the “mass” of air in the neck can be expressed as $\bar{\rho}L \dot{u}'_n = p'_1 - p'_2$. In this equation, $\bar{\rho}$ is the air density and u'_n is the bulk velocity of the incompressible-like oscillation of the air inside the neck. Visco-thermal losses will be discussed in a moment. For now, we use a general relationship between the acoustic velocity in the neck and the acoustic pressure difference, which reads in the frequency domain

$$Z_{vt}(\omega) \tilde{u}_n = \tilde{p}_1 - \tilde{p}_2 \quad (1)$$

where $Z_{vt}(\omega)$ is a frequency-dependent impedance of the neck. At the outer end of the neck, a significant amount of acoustic energy is lost through radiative effects, which can be expressed via a radiation impedance $Z_r(\omega)$:

$$Z_r(\omega) = \frac{\tilde{p}_2}{\tilde{u}_n}. \quad (2)$$

Gathering (1) and (2) yields $(Z_{vt} + Z_r)\tilde{u}_n = \tilde{p}_1$, and therefore

$$\frac{\Im(Z_{vt} + Z_r)}{\omega} \dot{u}'_n + \Re(Z_{vt} + Z_r)u'_n - p'_1 = 0 \quad (3)$$

Combining the mass conservation in the Helmholtz resonator volume and the linearized equation of state $p' = c^2 \rho'$ for isentropic fluctuations yields

$$\dot{p}'_1 = -\frac{\bar{\rho}c^2 S}{V} u'_n \quad (4)$$

Incorporating (4) into (3), one gets an ordinary differential equation for the acoustic pressure in the bottle:

$$\begin{aligned} \frac{\Im(Z_{vt} + Z_r)}{\omega} \dot{p}'_1 + \Re(Z_{vt} + Z_r) \dot{p}'_1 + \frac{\bar{\rho}c^2 S}{V} p'_1 &= 0 \\ \rho_0 L_{eq} \ddot{p}'_1 + \Re(Z_{vt} + Z_r) \dot{p}'_1 + \frac{\bar{\rho}c^2 S}{V} p'_1 &= 0 \\ \ddot{p}'_1 + \frac{\Re(Z_{vt} + Z_r)}{\bar{\rho}L_{eq}} \dot{p}'_1 + \frac{c^2 S}{VL_{eq}} p'_1 &= 0 \\ \ddot{p}'_1 + \alpha \dot{p}'_1 + \omega_0^2 p'_1 &= 0 \end{aligned} \quad (5)$$

where we have defined the corrected neck length

$$L_{eq} = \frac{\Im(Z_{vt} + Z_r)}{\bar{\rho}\omega}, \quad (6)$$

the acoustic damping coefficient

$$\alpha = \frac{\Re(Z_{vt} + Z_r)}{\bar{\rho}L_{eq}} = \omega \frac{\Re(Z_{vt} + Z_r)}{\Im(Z_{vt} + Z_r)}, \quad (7)$$

and the natural angular frequency

$$\omega_0 = c \sqrt{\frac{S}{VL_{eq}}}. \quad (8)$$

At the natural frequency ω_0 the visco-thermal impedance reads [1, 2]:

$$\begin{aligned} Z_{vt}(\omega_0) &= i\bar{\rho}\omega_0L \left[1 + (1-i)\frac{1}{R} \left(\delta_v + \delta_t(\gamma-1) \left(1 + \frac{2R_c}{L_c} \right) \right) \right] \\ &= i\bar{\rho}\omega_0L \left[1 + (1-i)\frac{\delta_v}{R} \left(1 + \frac{\gamma-1}{\sqrt{Pr}} \left(1 + \frac{2R_c}{L_c} \right) \right) \right] \end{aligned} \quad (9)$$

with $\delta_v(\omega) = \sqrt{2\nu/\omega}$ the thickness of the viscous boundary layer (Stokes boundary layer), $\delta_t(\omega) = \sqrt{2K/\bar{\rho}\omega C_p}$ the thickness of the thermal boundary layer, K the thermal conductivity, C_p the specific heat at constant pressure, γ the ratio of specific heats, $Pr = (\delta_v/\delta_t)^2 = \nu\bar{\rho}C_p/K$ the Prandtl number, and R_c and L_c the radius and length of the bottle cavity, respectively. This expression is valid for boundary layers that are thin compared to the neck radius, $\delta_v, \delta_t \ll R$, which is fully verified here: $\delta_v(\omega_0) \simeq 0.15$ mm, $\delta_t(\omega_0) \simeq 0.18$ mm $\ll R = 8.6$ mm. Viscous and thermal effects have a twofold contribution: dissipative and reactive. Indeed, they contribute both to (i) the acoustic damping (7) via the real part

$$\Re(Z_{vt}) = \frac{\bar{\rho}\omega_0L}{R} \left(\delta_v + \delta_t(\gamma-1) \left(1 + \frac{2R_c}{L_c} \right) \right), \quad (10)$$

and (ii) to corrections of the neck length (6) and natural angular frequency (8) via the imaginary part

$$\frac{\Im(Z_{vt})}{\bar{\rho}\omega_0} = L \left[1 + \frac{1}{R} \left(\delta_v + \delta_t(\gamma-1) \left(1 + \frac{2R_c}{L_c} \right) \right) \right]. \quad (11)$$

Conversely, in the limit of vanishing viscosity and thermal conductivity, the neck impedance reduces to $Z_{vt}(\omega_0) = i\bar{\rho}\omega_0L$; if in addition the radiation impedance $Z_r(\omega_0)$ is negligible, the acoustic oscillator (5) is undamped, $\alpha = 0$, and the neck length is uncorrected, $L_{eq} = L$, yielding the simplest model of Helmholtz resonator $\ddot{p}' + (c^2S/VL)p' = 0$.

The radiation impedance of a circular opening is [3, 4]:

$$Z_r(\omega_0) = \frac{\tilde{p}_2}{\tilde{u}_n} \simeq \bar{\rho}c \left[\frac{k_0^2 R^2}{4} + i0.61k_0R \right] \quad (12)$$

at low frequency (if $k_0R = (\omega/c)R \ll 1$, which is fully verified here: $k_0R = 0.033$). Therefore, like the neck impedance, the radiation impedance contributes both to the acoustic damping and to corrections of the neck length and natural frequency. Finally, from (6) and (9)-(12) we obtain the corrected length

$$L_{eq} = L \left[1 + \frac{1}{R} \left(\delta_v + \delta_t(\gamma-1) \left(1 + \frac{2R_c}{L_c} \right) \right) \right] + 0.61R. \quad (13)$$

Defining the neck length L for our bottle is not straightforward because its geometry features a smooth increase in radius, unlike the geometry of an ideal Helmholtz resonator with a sudden expansion separating a constant-radius neck and a constant-radius inner cavity (Fig. S1(a)). We define the neck length such that the peak frequency measured experimentally *without* jet (208 Hz) matches the natural frequency $f_0 = c\sqrt{S/VL_{eq}}/2\pi$ of an equivalent ideal Helmholtz resonator of same neck inner diameter $D = 2R$, same inner cavity volume $V(L)$ (total volume minus the volume occupied by the neck of length L), and same corrected neck length $L_{eq}(L)$. Solving this non-linear condition (Fig. S1(b)), we obtain numerically:

$$L = 41 \text{ mm}, \quad (14a)$$

$$\begin{aligned} L_{eq} &= L + \frac{L}{R} \left(\delta_v + \delta_t(\gamma-1) \left(1 + \frac{2R_c}{L_c} \right) \right) + 0.61R \\ &= 41 + 0.6 + 5.2 = 47 \text{ mm}, \end{aligned} \quad (14b)$$

$$\omega_0 = 2\pi \times 208 = 1307 \text{ rad/s}. \quad (14c)$$

We also obtain from (7) an estimation of the acoustic damping

$$\alpha = 36 \text{ rad/s} \quad (15)$$

that is in very good agreement with the value 35 rad/s obtained experimentally (Fig. S2) from the squared gain of the acoustic transfer function $H(\omega) = \tilde{p}_1/\tilde{p}_2$ (measured with a series of frequency sweeps performed with a loudspeaker located outside the bottle), either by calculating the quality factor directly (ratio $Q = \omega_p/\Delta\omega$ of the peak frequency to the full width at half maximum) or by fitting second-order low-pass or band-pass transfer functions. (Note that, without jet, the oscillator's natural frequency $\omega_0/2\pi$ and peak frequency $\sqrt{\omega_0^2 - \alpha^2/4}/2\pi$ are almost equal since $\alpha \ll \omega_0$.)

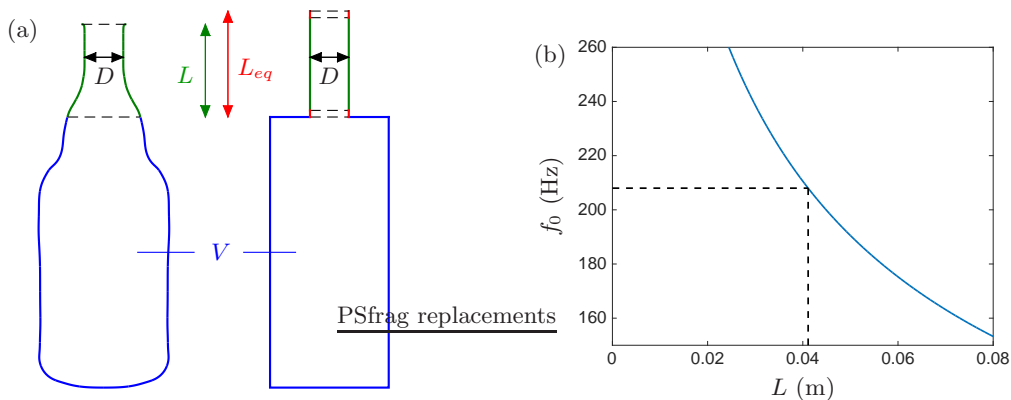


FIG. S1: (a) Sketch of the bottle (inner wall) and of an equivalent ideal Helmholtz resonator with sudden expansion. Both geometries are axisymmetric and have the same inner cavity volume V , neck inner diameter $D = 2R$, neck length L , equivalent neck length L_{eq} , and natural frequency $f_0 = c\sqrt{S/VL_{eq}}/2\pi$. (b) Variation with neck length L of the natural frequency $f_0 = c\sqrt{S/VL_{eq}}/2\pi$ of an ideal Helmholtz resonator of inner cavity volume V (excluding the neck region). The natural frequency $f_0 = 208$ Hz measured experimentally without jet corresponds to a neck length $L = 41$ mm.

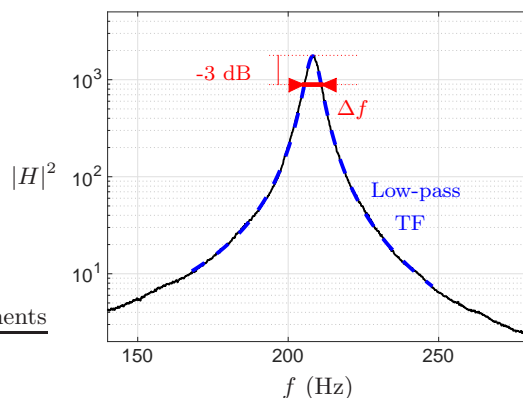


FIG. S2: Acoustic damping measurement with an external loudspeaker and no jet flow from the pipe. The bottle's *outside* \rightarrow *inside* acoustic transfer function H is reconstructed with cross-PSDs of time signals measured outside and inside the bottle during a series of frequency sweeps. The peak at $f_p = 208$ Hz has a quality factor measured directly as $Q = 37$ (red, ratio $f_p/\Delta f$ of peak frequency to width at half maximum), which yields an acoustic damping $\alpha = 2\pi f_p/Q = 35$ rad/s. A fit of $|H|^2$ with the squared gain of a second-order low-pass (blue) transfer function yields a damping value $\alpha = 36$ rad/s.

S2. DETERMINISTIC AND STOCHASTIC FORCING

When the acoustic oscillator (5) is forced by the impinging jet, this forcing has two components. First, a stochastic component is induced by turbulence, modelled here for simplicity as a white Gaussian noise $\xi(t)$ of intensity Γ , i.e. $\langle \xi \xi_\tau \rangle = \Gamma \delta(\tau)$. Second, a deterministic component is induced by coherent fluctuations in the jet. Several formulations based on the concept of vortex sound are well suited to describe this effect at low Mach numbers. For instance, Howe's analogy uses a potential flow as reference and defines an equivalent acoustic source accounting for the effect of vorticity (just as Lighthill's analogy uses a quiescent medium as reference and defines an equivalent acoustic source composed of viscous stresses, non-linear Reynolds stresses, and a non-isentropic term). Howe's analogy states that the force

$$\mathbf{f} = -\bar{\rho} \boldsymbol{\omega} \times \mathbf{u}, \quad (16)$$

with \mathbf{u} the total velocity field and $\boldsymbol{\omega} = \nabla \times \mathbf{u}$ the associated vorticity field, acts as an external forcing on the acoustic field, which is defined as the unsteady contribution of the potential component of the flow. This can be seen by comparing the expressions of Euler's equation in Crocco's form for a potential, inviscid, homentropic flow with

external forcing

$$\frac{\partial \mathbf{u}}{\partial t} + \nabla B = \frac{\mathbf{f}}{\rho} \quad (17)$$

and for a rotational flow without external forcing

$$\frac{\partial \mathbf{u}}{\partial t} + \nabla B = -\boldsymbol{\omega} \times \mathbf{u}, \quad (18)$$

where $B = |\mathbf{u}|^2 + \int dp/\rho$ is the total enthalpy, and $-\boldsymbol{\omega} \times \mathbf{u}$ is the Lamb vector. In fact, Howe's analogy becomes clear when deriving the associated wave equations: first, linearizing (17) at first order around a fluid at rest (in that case, $B' = p'/\bar{\rho}$ because $\bar{\mathbf{u}} = 0$), taking the divergence, subtracting the linearized equation for mass conservation ($\partial \rho'/\partial t + \bar{\rho} \nabla \cdot \mathbf{u}'$) and using the linearized equation of state ($p' = c^2 \rho'$) yields the wave equation for the acoustic pressure p' with dipolar volumetric forcing

$$\frac{1}{c^2} \frac{\partial^2 p'}{\partial t^2} - \nabla^2 p' = -\nabla \cdot \mathbf{f}'. \quad (19)$$

Second, multiplying Eq. (18) by ρ , taking the divergence, and using a series of manipulations as described in [5], one obtains

$$\left(\frac{D}{Dt} \left(\frac{1}{c^2} \frac{D}{Dt} \right) - \frac{1}{\rho} \nabla \cdot (\rho \nabla) \right) B = \frac{1}{\rho} \nabla \cdot (\rho \boldsymbol{\omega} \times \mathbf{u}),$$

where D/Dt is the material derivative. For low-Mach source regions, the ratio of local density and speed of sound to their mean values is given by $1 + O(M^2)$, where M is the Mach number. Therefore, at first order and neglecting nonlinear advection terms in the material derivatives, we obtain

$$\frac{1}{c^2} \frac{\partial^2 B'}{\partial t^2} - \nabla^2 B' = \bar{\rho} \nabla \cdot (\boldsymbol{\omega} \times \mathbf{u})'. \quad (20)$$

This is a wave equation for the fluctuations of the total enthalpy, which, together with Eq. (19), leads the analogy established by Howe. Indeed, if in the far field $\boldsymbol{\omega}$ and \mathbf{u} vanish, we retrieve from Eq. (20) the wave equation for p' . In the present situation, the flow region where the vorticity interacts with the acoustic field is localized at the neck opening. It is therefore interesting to evaluate the production or absorption of acoustic energy related to the work of the force (16) along the central plane of the neck of the bottle:

$$\mathcal{P}(x, t) = \int \mathbf{f}' \cdot \mathbf{u}_{ac} dy = -\bar{\rho} \int (\boldsymbol{\omega} \times \mathbf{u}') \cdot \mathbf{u}_{ac} dy. \quad (21)$$

Note that since the acoustic velocity \mathbf{u}_{ac} is harmonic in time and of zero mean, the mean component of \mathbf{f} does no work, and only its fluctuating component \mathbf{f}' contributes to \mathcal{P} as expressed in Eq. (1) of the main article.

The force (16) is clearly a non-linear function of the velocity field \mathbf{u} , which itself depends non-linearly on the acoustic field: the shear layer above the neck amplifies disturbances, generating coherent hydrodynamic fluctuations in a preferred range of frequencies; as the amplitude of these disturbances increases, coherent fluctuations modify the mean flow: typically, the shear layer widens and vorticity weakens, resulting in a smaller amplification. We model this saturation process with a non-linear damping of the simplest form,

$$-\nabla \cdot \mathbf{f}' = \frac{1}{c^2} (\beta - \kappa p_1'^2) p_1', \quad (22)$$

with $\beta > 0$, $\kappa > 0$.

Finally, combining the acoustic oscillator (5), the wave equation (19), the non-linear hydrodynamic forcing (22), and adding a stochastic term $\xi(t)$ accounting for the jet turbulence, the aero-acoustic system reads

$$\ddot{p}_1' + \omega_0^2 p_1' = (\beta - \alpha - \kappa p_1'^2) p_1' + \xi(t) \quad (23)$$

which corresponds to a stochastic Van der Pol oscillator (Eq.(2) of the main article) with linear growth rate $\nu = (\beta - \alpha)/2$.

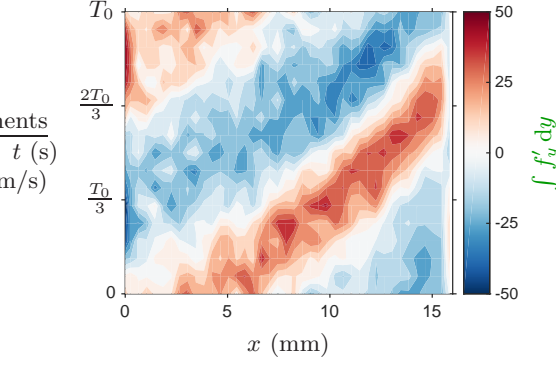


FIG. S3: Space-time evolution of $\int f'_y dy$, vertical component of the fluctuating acoustic force integrated vertically at each streamwise location.

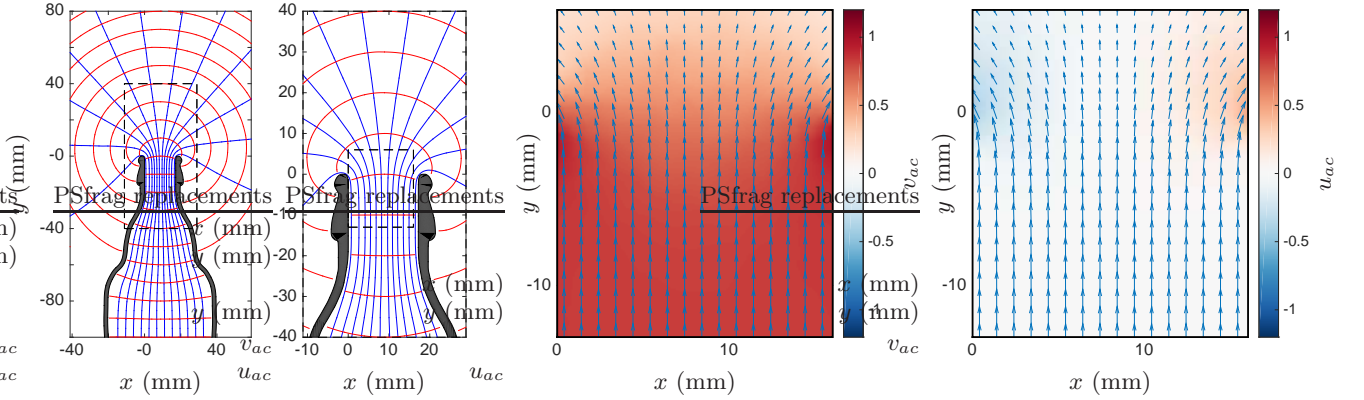


FIG. S4: Dominant acoustic mode computed with a linear Helmholtz solver. (a) Equipotentials (red) and streamlines (blue) in the symmetry plane $z = 0$, showing the structure of a compact monopole. (b) Vertical and horizontal velocity fields in the same plane. Here the linear mode is normalized such that the largest acoustic velocity magnitude is 1.

S3. EXAMPLE OF SPATIO-TEMPORAL EVOLUTION OF THE ACOUSTIC FORCING

Figure 1(c) of the main article shows a two-dimensional estimation of the acoustic power density (21) using vertical projections of the force $\mathbf{f}' \cdot \mathbf{e}_y$ and of the acoustic velocity $\mathbf{u}_{ac} \cdot \mathbf{e}_y$, from phase-averaged experimental measurements in the symmetry plane $z = 0$. For completeness, Fig. S3 shows the vertical component of the force (*without* projection onto \mathbf{u}_{ac})

$$f'_y = \mathbf{f}' \cdot \mathbf{e}_y = -\bar{\rho}(\boldsymbol{\omega} \times \mathbf{u})' \cdot \mathbf{e}_y \simeq -\bar{\rho}(\omega_z u_x)', \quad (24)$$

integrated vertically across the jet along y . The force exhibits a clear wave structure in the streamwise direction x (with one wavelength across the neck), and spatio-temporal propagation downstream at about 3 m/s, which is substantially smaller than the jet velocity at the pipe termination (22 m/s). The spatial distribution of the acoustic velocity field \mathbf{u}_{ac} which is used for the evaluation of $\mathcal{P}(x, t)$ is computed using a Helmholtz solver (see Fig. S4), and the temporal evolution is adjusted based on the PIV data at the bottom left corner of the field of view which is vorticity-free all along the acoustic cycle.

S4. VALIDATION OF THE PARAMETER IDENTIFICATION USING CONTROLLED TRANSIENTS

The output-only parameter identification method is well-suited for stochastic systems that cannot be controlled; here we take advantage of the fact that the aeroacoustic system can be controlled with an acoustic forcing and quantitatively validate the identification results. In this second set of experiments, we add an external loudspeaker 20 cm away from the bottle neck, and proceed as follows. First, for linearly stable conditions (U, θ) , the loudspeaker

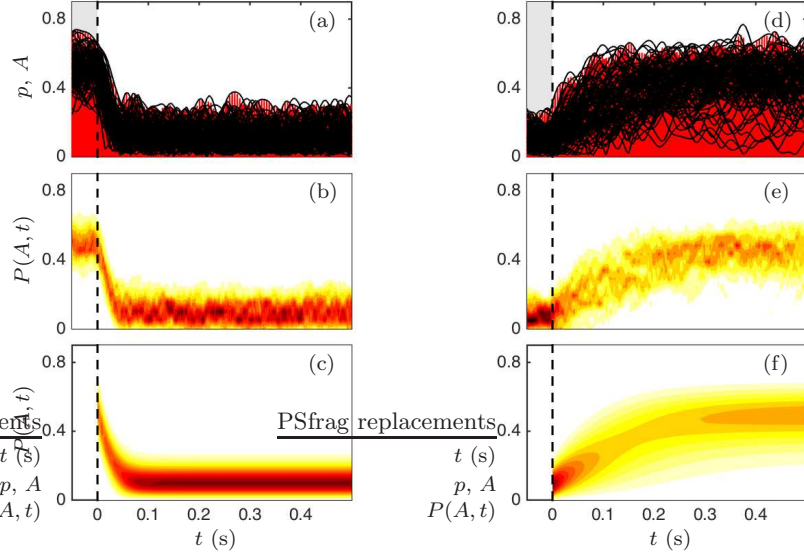


FIG. S5: Transient relaxation dynamics when control from an external loudspeaker is turned off. (a,d) envelope A (black) of the acoustic pressure p (red) from 100 experimental realizations. (b,e): evolution of the probability density (ensemble average of the envelopes in (a,d) at each time instant). (c,f): evolution of $P(A, t)$ from the FPE solved in time with the experimental PDF at $t = 0$ and with the parameters ν , κ , Γ from the adjoint-based identification. Conditions (gray triangles in main Fig. 2(b)): $U = 18$ m/s, (a) $\theta = 20^\circ$ (linearly stable, relaxation to low-amplitude fluctuations), and (b) $\theta = 35^\circ$ (linearly unstable, relaxation to a large-amplitude limit cycle).

imposes a constant-amplitude forcing at frequency f_a ($t < 0$ in Fig. S5(a)). At $t = 0$, the forcing is switched off and the system relaxes to its uncontrolled natural state: a stochastically driven linear oscillator. Second, for linearly unstable conditions (U, θ), a feedback control is applied to suppress the limit cycle ($t < 0$ in Fig. S5(d)), based on a real-time controller (NI cRIO-9066) coded to delay and amplify the acoustic pressure signal, and to feed the loudspeaker. By adjusting the time delay, it is possible to suppress the large-amplitude aeroacoustic limit-cycle. At $t = 0$, the control is switched off and the system is free to relax to its stable stochastically forced limit cycle. In each case, we repeat 100 independent realizations (Fig. S5(a), (d)), and compute the ensemble-averaged evolution in the forced/controlled stationary regime and unforced/uncontrolled transient regime (Fig. S5(b), (e)). Next, we solve the FPE numerically in time (see numerical method in [6]), starting from $P(A, 0)$ experimentally measured at $t = 0$, and using the values of ν , κ , Γ from the adjoint-based identification (Fig. S5(c), (f)). The time evolution of $P(A, t)$ obtained numerically is closely aligned with its experimental counterpart, which validates the parameter identification and the stochastically-forced VdP model.

* eboujo@ethz.ch

† noirayn@ethz.ch

- [1] R. F. Lambert, The Journal of the Acoustical Society of America **25**, 1068 (1953).
- [2] G. Searby, M. Habiballah, A. Nicole, and E. Laroche, Journal of Propulsion and Power **24**, 516 (2008).
- [3] H. Levine and J. Schwinger, Physical Review **73**, 383 (1948).
- [4] A. Chaigne and J. Kergomard, *Acoustics of Musical Instruments*, Modern Acoustics and Signal Processing (Springer, New York, NY, 2016).
- [5] M. Howe, *Theory of Vortex Sound* (Cambridge University Press, New York, 2002).
- [6] E. Boujo and N. Noiray, Proceedings of the Royal Society A: Mathematical, Physical and Engineering Science **473** (2017).